*energies*

MDPI

*Article*

# Theoretical Analysis Based on Experimental Studies of Heat and Moisture Fluxes Penetrating Through a Masonry Wall Above Ground Level in an Annual Cycle

**Mariusz Owczarek [1,*] and Barbara Nasiłowska [2]**

[1] Faculty of Civil Engineering and Geodesy, Military University of Technology, gen. Sylwestra Kaliskiego Street 2, 00-908 Warsaw, Poland
[2] Institute of Optoelectronics, Military University of Technology, gen. S. Kaliskiego 2, 00-908 Warsaw, Poland; barbara.nasilowska@wat.edu.pl
* Correspondence: mariusz.owczarek@wat.edu.pl

**Abstract:** This article calculates horizontal and vertical heat and moisture fluxes in the wall based on measurements of temperature and relative humidity in the building wall. It was a basement wall that was close to the ground on one side and the basement ceiling on the other, which increased the difficulty in problem simulation. The brick material from the wall was also analyzed under an electron microscope and its elemental composition was determined using the EDX (Energy Dispersive X-ray spectroscopy) method. The brick had a relatively uniform elemental composition apart from several variations in calcium content. Monthly, daily, and hourly heat and moisture fluxes were determined. The tested wall was characterized by low humidity, and the values obtained of the moisture fluxes confirmed this. The maximum recorded relative humidity inside the wall is 57.89%, and the minimum is 43.99%. The effect of buffering moisture by brick material was noticed. Vertical streams of water vapor were found to be important in the moisture balance of the tested partition. The maximum heat flux through the tested wall area in August was 0.06 W, and the minimum in January was −0.2 W. The maximum moisture flux in August was $5 \times 10^{-11}$ kg/s, and the minimum in January was $-5 \times 10^{-11}$ kg/s.

**Keywords:** moisture content; masonry wall; heat fluxes; porous material vapor conductivity; temperature and humidity measurements



**Citation:** Owczarek, M.; Nasiłowska, B. Theoretical Analysis Based on Experimental Studies of Heat and Moisture Fluxes Penetrating Through a Masonry Wall Above Ground Level in an Annual Cycle. *Energies* **2024**, *17*, 5687. https://doi.org/10.3390/en17225687

Academic Editor: Andrea Frazzica

Received: 21 October 2024
Revised: 9 November 2024
Accepted: 11 November 2024
Published: 14 November 2024



## 1. Introduction

The transfer of heat and moisture through the building envelope has a significant impact on energy demand and the condition of the partitions. It is taken into account in both legal requirements for buildings and energy calculation algorithms. Research on this topic can be carried out under laboratory or real conditions, through simulation or measurement. Knowledge of heat and moisture fluxes enables the correct design of building insulation; the impact of insulation moisture on its effectiveness was described in [1], and the inclusion of capillary water in simulations of the building envelope was studied in [2]. It is also very important in the renovation of historic buildings, where moisture is one of the basic factors affecting masonry structures [3]. Precise thermal and humidity simulations require the determination of many boundary parameters of the partition analyzed. If it is not possible to obtain these properties from measurements for a specific material, an extensive literature analysis is required, as was conducted in [4,5].

Heat and moisture transfer are often described as one-dimensional, and such calculations are performed in HAM analysis programs such as WUFI [6], HAM-Tools [7], and Delphin [8]. However, a theoretical analysis of this type may not be sufficient for walls with a heterogeneous structure, e.g., near ceilings, the ground, and other variable boundary conditions on the surface, such as local shading and sunlight. By taking into

account heat flow in two or three dimensions, it is possible to capture phenomena that are omitted in a one-dimensional approach. Kosny et al. [9] presented the results of research on frame technology walls modeling, proving that the one-dimensional approach can lead to significant errors. In order to estimate the risk of mold growth, dos Santos and his team [10] examined the heat and moisture flow in the wall close to the ceiling. These studies showed that for two-dimensional analysis, smaller errors and more accurate results were obtained.

In a wall with a homogeneous layered structure, two-dimensional heat flow may also occur, for example, in the case of variable exposure to solar radiation [11]. The heat flux directed along the height of the wall can change not only its value but also its direction. Taking into account multidimensional heat and moisture flows requires the use of complex computational processes. Therefore, simplification methods are sought for "whole building" simulations [12]. These simulations did not take into account the exchange of heat and moisture with the ground, which was associated with an increase in costs. In the case of Takada et al. [13], although they simulated a wall in contact with the ground, their simulation was one-dimensional. Moisture in the wall is important due to the thermal and humidity conditions inside the building. The wall material acts as a buffer layer for moisture, reducing its dependence on the external environment—this issue was the subject of IEA-ECC Annex 41 [14].

Determining vertical flows is particularly important for places in the building envelope, such as the proximity of ceilings or walls buried in the ground. Therefore, complementing the existing state of knowledge, this article presents research on horizontal and vertical heat and moisture flows passing through a masonry wall above ground level in not only annual but also monthly, daily, and hourly cycles. The results in the monthly cycle illustrate the flow on a larger scale, while the shorter time step aims at a more detailed analysis of the components of the total flows. The analysis presented in this article can be used to validate theoretical models.

To measure the heat flux, many researchers use heat flux meters [5,15]. This approach gives accurate results but allows for measuring fluxes only on the wall surface, and HFM (heat flux meter) sensors are expensive and susceptible to damage. An alternative is to measure temperatures and to know the thermal resistance between them. This method is called ASTR (Air-Surface Temperature Ratio) [16]. In the simplest case, the heat flux is determined from the wall surface temperature, the air temperature on the same side, and the heat transfer coefficient on the surface. Obtaining reliable values of the heat transfer coefficient on the surface for a specific task is difficult. To overcome this, the inverse heat conduction problem (IHCP) is used and the heat flux is determined by minimizing the difference between the calculated and measured temperatures inside the body. A review of the literature on this topic is given in [17]. This article proposes a method based on measuring the temperatures inside the wall and knowing the conduction resistance between them. Conduction resistance is a material property that can be obtained more easily for a given material than the heat transfer coefficient, which depends on many external factors. A heat flux from the wall surface as in the typical ASTR method was not obtained, but measurement close to its surface can be conducted. This method was also adapted to measure the moisture flux. In this case, instead of calculations, they are based on measurements of the initial water vapor pressure and the vapor conductivity coefficient.

Heat flux measurements can be performed to determine the thermal parameters of the wall or to estimate the energy flowing through the wall. A masonry wall can be modeled with varying degrees of precision as a homogeneous material or as a brick and mortar. In [18], the thermal properties of bricks and mortar were determined by comparing theoretical relationships and temperature measurements at various depths. The wall model was made up of electrical resistances corresponding to the wall components. The heat flux was calculated using the basic formulas from the Fourier equation, similarly to this article. The thermal properties of hollow bricks with different geometries were considered in [19]. The authors investigated the brick response time (BRT), which describes the thermal inertia behavior based on simulations of bricks with three internal structures. In [20], the behavior

of earth brick walls was investigated and the results obtained indicate a very good ability to regulate humidity in rooms due to such walls. In publication [21], the humidity level in the wall was examined during intense humidification corresponding to the rain shower, using measurements of relative humidity inside the partition in the place of bricks and mortar. Large humidity increases were achieved, from 25% to more than 90% in an hour. After protecting the wall with a waterproofing layer, a greater insulating effect was achieved on the mortar than on the brick. It seems that, in general research, there is a problem in distinguishing moisture from capillary water and water vapor by measurement. Such a distinction would improve the description of moisture flow in building materials.

What is new in this approach is the determination of the heat and moisture fluxes inside the wall. Under unsteady conditions, these fluxes are not equal to the flux at the surface. It is not possible to place a heat flow meter or even more a moisture flow meter inside the wall. Meanwhile, moisture flow is important to determine the sources of wall moisture. The heat flow, on the other hand, answers the question of energy storage in the wall and the influence of solar radiation and internal and external temperatures. Dondi et al. in the publication [22] presented correlations between water vapor permeability and the main elemental composition and microstructure of 13 types of bricks. They observed an increase in water vapor permeability with increasing brick porosity.

## 2. Materials and Methods

This section presents the methods used, divided into testing the structure of the material and the flow of heat and moisture. The devices and characteristics of the wall material were presented.

### *2.1. Structural Tests of Wall Material*

The properties of materials are determined by their structure, so direct observation is important in explaining the phenomena occurring in them. Electron microscopy and chemical analysis can be used to reveal the internal structure of building materials [23,24]. Structural studies were performed using a Quanta 250 FEG FEI scanning electron microscope (Quanta 250 FEG SEM, FEI, Hillsboro, OR, USA) coupled with a backscattered electron detector (ETD-BSE, FEI, Hillsboro, OR, USA) with an accelerating voltage of 10 kV, spot 3. In order to improve the imaging quality of nonconductive brick samples, a 7 nm gold layer was deposited using a high-vacuum EM ACE 600 sputter (Leica Microsystems, Wetzlar, Germany). During the spraying process, the table rotated at an angle of 120°.

The chemical composition of the brick was examined using a Quanta 250 FEG FEI scanning electron microscope (Quanta 250 FEG SEM, FEI, Hillsboro, OR, USA) coupled with an EDX (Energy Dispersive X-Ray Analysis) detector made by the same manufacturer. The following parameters were used during the EDX analysis: spot 4.5, 30 kV.

### *2.2. Measuring Station—External and Internal Conditions*

The internal room of the tested facility is part of the basement with an area of 35 $m^2$, with low ventilation and little sunlight, which is possible due to the presence of four windows measuring 0.55 × 0.5 m. In one of the external walls, facing SE, a temperature and humidity measurement stand was installed, consisting of sensors inside its structure and outside and inside the room. Measurements were performed using the devices listed in Table 1.

The external temperature and humidity probes were placed in an instrument shelter. The total thickness of the wall made of solid ceramic brick was 0.6 m. The height of the wall was 2.5 m. On the outer side, up to the level of 1.78 m, the wall was in contact with the ground and the remaining part of the wall, which was 0.72 m, was exposed to the direct influence of environmental conditions and atmospheric air. The part in contact with the ground had thermal and humidity insulation made during the renovation in 2023. Thermal insulation consisted of 10 cm of polystyrene, while moisture insulation consisted of a bituminous layer and a high-density polyethylene membrane. Therefore, it can be

assumed that the moisture from the ground penetrated the lower uninsulated surface of the foundations.

**Table 1.** Data on measuring devices in the described wall.

| Function | Name | Description |
| --- | --- | --- |
| Data logger | Wi-MA2D0A0 (APONE, Poznań, Poland) | Measuring device interface RS-485 (Modbus RTU) PC Interface RS-485 (Modbus RTU) Memory: SD card max. 4 GB |
| Temperature/ humidity in the wall and inside the room | SiOne Si-S00WRA0 (APONE, Poznań, Poland) | Temperature: Measuring range: −30 ÷ +60 °C Accuracy: ±0.2 °C Relative humidity: Measuring range: 0 ÷ 100% Accuracy: max. ±2.0% RH |
| Relative humidity and temperature probe in external environment | Sens-H-S3 (APONE, Poznań, Poland) | Probe for meteorological applications Temperature: Measuring range: −50 ÷ 100 °C, Accuracy: ±0.1 K Relative humidity: Measuring range: 0 ÷ 100% Accuracy: max. ±0.8% RH |
| Air temperature/humidity transmitter for the Sens-H-S3 probe | Si-H00C5A0 (APONE, Poznań, Poland) | Measuring range: depends on the probe Accuracy: depends on the probe |

For identification purposes, the measurement points were marked with numbers. These numbers come from the point coordinate, with the points between which horizontal streams are calculated being marked with the $x$ coordinate, and the points for vertical stream calculations being marked with the $y$ coordinate. The geometry, coordinate system, and sensor installation points are marked with red points, and their numbering in the wall cross-section is shown in Figure 1. The wall is treated as homogeneous, i.e., the thermal conductivity and water vapor permeability coefficient takes into account both brick and mortar. Better estimation of mortar parameters is a problem that will need to be solved in further research, as there are no appropriate mortar samples for testing.

It was assumed that the temperature was constant along the $z$ axis, i.e., along the wall. Measuring points at depths along the $x$ axis are shifted relative to each other for technical reasons, creating the main row of sensors, but are treated as if they were on one axis. For the $y$-axis direction, the measurement possibilities are limited because above and below the main row of sensors there is only one measuring point at $x$ = 0.35 m, so the measured flux is the flux in the core of the wall cross-section. A photo of the measuring station is shown in Figure 2, and a 3D view of the measurement area and surfaces normal to the measured streams is shown in Figure 3.

The external dimensions of the wall and the fact that it is made entirely of solid brick are known. The removal of the outer layer during renovation revealed an inaccurate filling of some joints, but the exact distribution of the defects is unknown. The wall is about 100 years old and the entire building is historic, so it was not possible to perform invasive wall tests. Horizontal sensors were placed symmetrically in relation to the wall axis, and vertical sensors were placed symmetrically in relation to vertical sensors. A certain problem is the variability of color and therefore the absorption of solar radiation between the tiles and the plaster.

It was assumed that the temperature value read by the sensors is representative at a distance of 0.05 m from the sensor horizontally and 0.07 m from the sensor vertically. For

such a sensor spacing, the dimensions of the plane normal to the heat and moisture flux were calculated. The area $A_x$ perpendicular to the heat flow along the $x$ axis $q_x$ is

$$A_x = 0.3 \times 0.16 = 0.048 \text{ m}^2 \quad (1)$$

and $A_y$ to the flow along the $y$-axis $q_y$ is

$$A_y = 0.1 \times 0.1 = 0.01 \text{ m}^2 \quad (2)$$

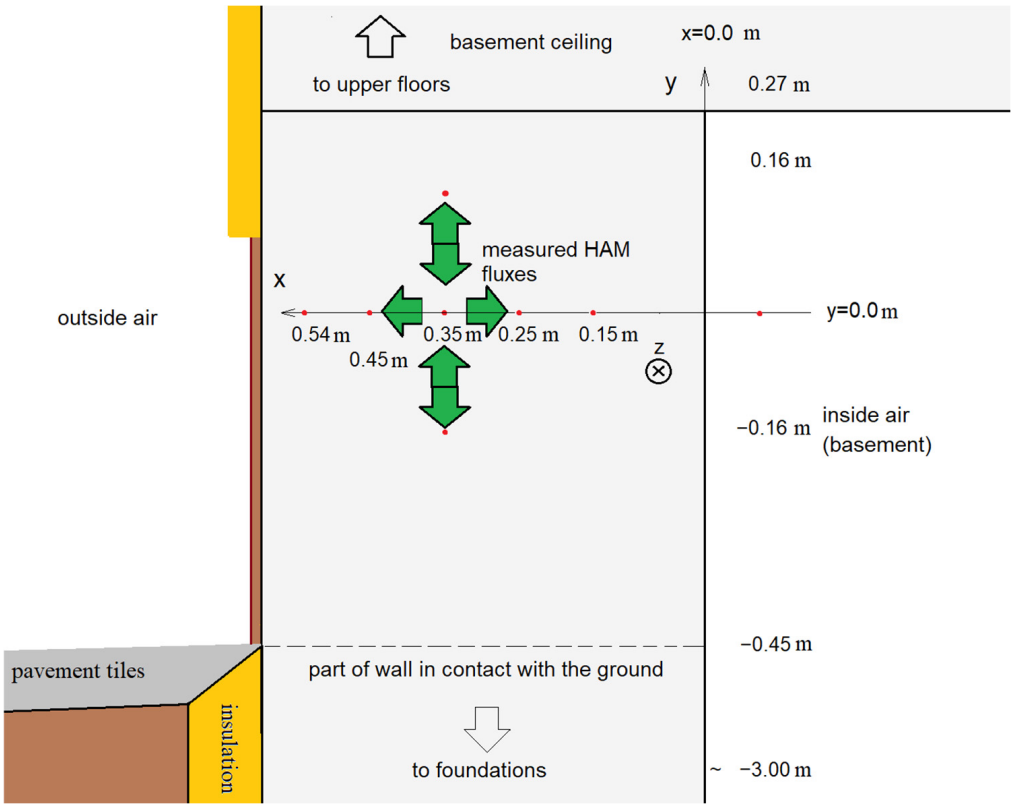


**Figure 1.** Geometry and coordinate system of the analyzed wall fragment. Red dots indicate temperature and humidity sensors, green arrows indicate determined heat and moisture fluxes.


**Figure 2.** Photos of the measurement station: (**a**) external conditions sensors, (**b**) sensor holes in the wall.

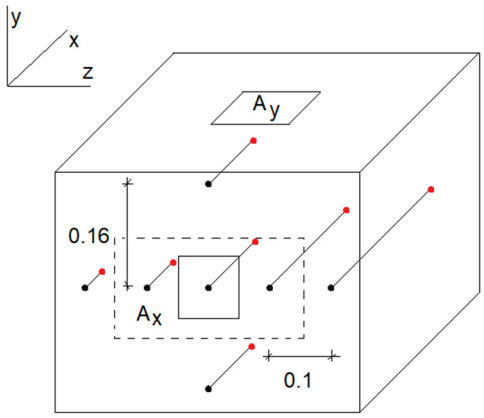


**Figure 3.** Surfaces normal to the measured heat flux. Red dots indicate temperature and humidity sensors, black dots are starting holes for the channels in which the sensors were placed.

The flux $q_x$ is therefore the real flux through the area $A_x$ of the wall, while $q_y$ is the flux only through the center of its cross-section. The $A_x$ surfaces were limited to the square marked with a solid line to enable mutual quantitative comparison of these streams; such a change of surface does not change the presented task conditions. In this way, a balance of heat and moisture fluxes was obtained for a cube inside the wall located at the intersection of cuboids with bases $A_x$ and $A_y$. The flow $q_x$ is expected to correspond to the flows between the inner and outer spaces. The $q_y$ flux depends on the thermal state of the connection between the wall and the basement ceiling and the exchange of heat and moisture with the ground.

### *2.3. Thermal and Humidity Properties of the Wall Material*

#### 2.3.1. Heat Conduction Coefficient

The heat conduction coefficient depends on humidity. This relationship is, among other things, related to the effect of evaporation and condensation of water, which causes the transfer of latent heat. In the work of Gawin et al. [25], it was shown that the effect of moisture on the apparent heat conduction coefficient can be described by a linear relationship.

The relationship between the thermal conductivity coefficient and the brick from the wall tested was determined by measurements at known humidity. Measurements were made using the transient method using the Isomet 2114 device (Applied Precision, Bratislava, Slovakia). Humidity values were measured for 4 states (Table 2). State I of brick humidity was after 48 h in a vacuum dryer at 120 °C, state II corresponded to humidification in atmospheric air for 48 h, and states III and IV occurred after exposure to liquid water for 24 and 48 h, respectively.

**Table 2.** Results of measurements of the thermal conductivity coefficient depending on humidity.

| Parameter | State I (Dry) | State II | State III | State IV |
|---|---|---|---|---|
| Humidity [%] | 0 | 1.55 | 15.48 | 22.85 |
| Humidity [kg/kg] | 0 | 0.0155 | 0.1548 | 0.2285 |
| Humidity [kg/m$^3$] | 0 | 23.77 | 237.33 | 350.24 |
| λ [W/mK] | 0.42 | 0.49 | 1.05 | 1.29 |

The relationship is linear, for humidity expressed in kg/m$^3$, and it was approximated by the equation:

$$\lambda_m(w) = 0.0025w + 0.4293 \quad (3)$$

where $\lambda_m$ $(w)$—thermal conductivity coefficient of the brick [W/(mK)], and $w$—brick humidity [kg/m$^3$].

For humidity in kg/kg for comparison with [25]

$$\lambda_m(w) = 3.8437w^* + 0.4293 \quad (4)$$

where $w^*$ brick humidity [kg/kg].

2.3.2. Water Vapor Permeability

Water vapor permeability $\delta_m$ was assumed as for brick no. 4 from [26] because it has a similar moisture content in the state of capillary saturation $w_{cap}$ = 316 kg/m$^3$, with the tested brick being 384 kg/m$^3$. The relationship between water vapor permeability and relative humidity φ is presented in Table 3.

**Table 3.** Assumed dependence of water vapor permeability $\delta_m$ on relative humidity $\varphi_m$ [26].

| $\varphi$ [-] | 0.1 | 0.2 | 0.3 | 0.4 | 0.5 | 0.6 | 0.7 | 0.8 | 0.9 | 1.0 |
|---|---|---|---|---|---|---|---|---|---|---|
| $\delta_m$ $10^{-12}$[kg/(m × s × Pa)] | 3.04 | 3.15 | 3.26 | 3.37 | 3.48 | 3.60 | 3.73 | 3.86 | 3.99 | 4.13 |

The plot of the data from Table 3 in the graph shows the linear nature of the relationship between vapor permeability and relative humidity, so a linear function was adopted to approximate it.

$$\delta_m(\varphi) = 1 \times 10^{-12} \times \varphi + 3 \times 10^{-12}. \quad (5)$$

2.3.3. Sorption Isotherm

Calculating the thermal conductivity coefficient requires knowledge of the moisture content of the material. Because the measured quantity is relative to air humidity, the moisture content of the material was determined on the basis of the sorption isotherm. The shape of the isotherm was adopted according to the research of Garbalińska and Siwińska [27] as for ceramic brick. It was approximated by the Chen equation:

$$w_{i\%}(\varphi) = \frac{a\varphi}{(1 + b\varphi)(1 - c\varphi)} \quad (6)$$

where the coefficients for ceramic brick at 20 °C $a$ = 0.041609, $b$ = 1.923164, $c$ = 1.006998, $w_{i\%}$ mean the moisture content in [%]. The shape of the curve was checked for a brick obtained from the analyzed wall by measuring one point of the sorption isotherm in a climatic chamber. For humidity $\varphi$ = 0.95, after moistening to a constant mass, the brick moisture content $w_{i\%}$ = 0.46% was obtained, while the equation obtained $w_{i\%}$ = 0.42%, which is in very good agreement. The tabularized values from Equation (6) are presented in Table 4.

**Table 4.** Assumed dependence of brick moisture content $w_{i\%}$ on relative humidity $\varphi_m$ [27].

| $\varphi$ [-] | 0.2 | 0.4 | 0.6 | 0.8 | 0.9 | 0.99 |
|---|---|---|---|---|---|---|
| $w_{i\%}$ [%] | 0.0075 | 0.0158 | 0.0293 | 0.0675 | 0.1463 | 4.6176 |

*2.4. Determination of Heat Fluxes*

In further considerations, the measurement points for shortening are marked with a vertical or horizontal coordinate. Thus, the point with coordinates (0.35;0) was marked "0.35", and the point (0.35;0.16) was marked "0.16". The heat flux between point $i$ and $j$ was calculated using Fourier's equations

$$q_{h,i,j} = A_{x,y} \frac{\lambda_m(w)(T_i - T_j)}{\Delta x_{i,j}} \quad (7)$$

where $T_i$, $T_j$ are the temperatures at the individual measurement points marked with their $x$ or $y$ coordinates as in Figure 1, $\Delta x_{i,j}$ means the distance between point $i$ and $j$, and $A_{x,y}$ means $A_x$ for the horizontal stream or $A_y$ for vertical. The moisture flux indices were written on the same principle. All streams are oriented relative to the "0.35" node. For example, $q_{h,0.25,0.35}$ is the heat flow between nodes "0.25" and "0.35", and a positive value means the flow towards node "0.35". Table 5 shows the signs of the flows relative to the sides of the wall. This classification is useful for describing the direction of heat flow in the analysis of energy losses and gains in the building.

**Table 5.** Signs of heat fluxes relative to the sides of the wall.

| **Stream Direction** | | |
|---|---|---|
| Horizontal | (room → external air) | (external air → room) |
| $q_{h,0.25,0.35}$ | positive (+) | negative (−) |
| $q_{h,0.45,0.35}$ | negative (−) | positive (+) |
| Vertical | (upper floors → foundations) | (foundations → upper floors) |
| $q_{h,-0.16,0.35}$ | negative (−) | positive (+) |
| $q_{h,0.16,0.35}$ | positive (+) | negative (−) |

### *2.5. Determination of Moisture Fluxes*

The moisture stream in the material penetrates due to two mechanisms: water vapor and capillary water. At lower humidity values, the water vapor transfer mechanism dominates, and at higher humidity values, capillary moisture prevails. In the research described in [28], ceramic brick is characterized by a pore distribution with a single maximum of macropores and a small number of them outside of this area. With such a structure, moisture transfer in the hygroscopic range takes place mainly by water vapor transport, and only when the humidity of the surrounding air approaches saturation does the share of capillary water flow rapidly increase. Since the maximum recorded relative humidity was approximately 65%, the share of liquid phase transport is small [29,30], and therefore they were omitted.

The steam flow was calculated using Fick's first law, as follows:

$$q_{v,i,j} = A_{x,y} \frac{\delta_m(\varphi)(p_{vi} - p_{vj})}{\Delta x_{i,j}}, \tag{8}$$

where $p_{vi}$, $p_{vj}$ are the partial pressures of vapor at points $i$,$j$. Partial pressures were determined on the basis of the simultaneous measurement of temperature and relative humidity.

The signs of the streams relative to the sides of the wall are the same as in Table 2.

### *2.6. Monthly Energy and Moisture Flows*

The monthly energy flows $E_{i,j}$ were calculated by summing the products of the flows $q_{h,i,j}$ and the measurement time step $\Delta t$ [s] for the entire month.

$$E_{i,j} = \sum_{n=1}^{k} q_{h,i,j} \Delta t, \tag{9}$$

Additionally, horizontal flows were compared with flows calculated using the steady-state method as in the monthly method of calculating the energy demand for the building.

$$E_{ss} = A_x \frac{\lambda_m}{d} (T_{int} - T_{ext}) t_m, \tag{10}$$

The thermal conductivity coefficient was calculated for a humidity of 3.75 kg/m$^3$, $\lambda_m$ = 0.439 W/(mK), because this is the humidity in the middle of the hygroscopic range, the $T_{int}$ and $T_{ext}$ temperatures are the average internal and external temperatures in the

month, d = 0.6 m is the thickness of the wall, and tm means the duration of the month [s]. For August, $T_{int}$ = 24 °C and $T_{ext}$ = 22.1 °C, and for January, $T_{int}$ = 22.6 °C and $T_{ext}$ = −0.8 °C.

The monthly moisture flows from measurements were calculated similarly:

$$G_{i,j} = \sum_{n=1}^{k} q_{v,i,j} \Delta t. \tag{11}$$

And for comparison, using the stationary method from the formula:

$$G_{ss} = A_x \frac{\delta_m}{d} (p_{int} - p_{ext}) t_m \tag{12}$$

The water vapor conductivity coefficient was calculated for a relative humidity of 50%, $\delta_m = 3.5 \times 10^{-12}$ kg/(m × s × Pa), and the partial pressures of water vapor $p_{int}$ and $p_{ext}$ are the average internal and external values in the month. For August $p_{int}$ = 1774 Pa and $p_{ext}$ = 1769 Pa, and for January $p_{int}$ = 765 Pa and $p_{ext}$ = 518 Pa.

The methodology used in this study is presented in Figure 4. Based on the measurements of external conditions, January and August were selected to calculate instantaneous heat and moisture fluxes. Instantaneous fluxes were calculated for each measurement in these months. Then, the average daily fluxes were calculated by averaging the instantaneous ones. Monthly fluxes were calculated by adding the energy exchanged at subsequent time steps over a month. The numerical procedure is explained further in Figure 5.

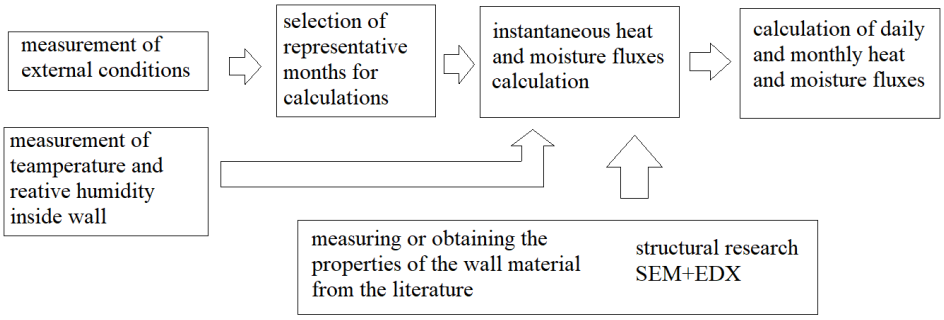


**Figure 4.** Methodology used in this study.

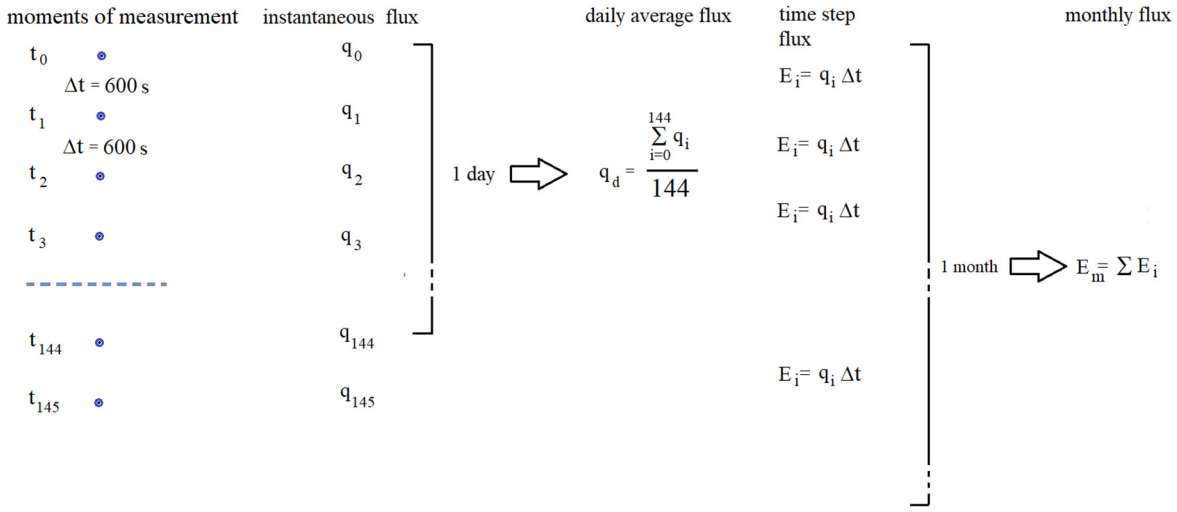


**Figure 5.** Numerical procedure used in this study.

### *2.7. Uncertainty Analysis*

The external and internal temperature measurement chain consists of a temperature sensor that, according to the manufacturer, has accuracy according to Table 1. The external

sensor is placed in the Rotronic AC1000 (Rotonic AG, Bassersdorf, Switzerland) weather cover, providing protection against wind up to a speed of 70 m/s and falling rain. The internal temperature sensor is located approximately 2 cm from the wall, so its readings may be influenced by the wall layer. The sampling period is 10 min. The uncertainty in the measurement of heat and humidity fluxes in the wall depends on the precision of the probes in Table 1, the uncertainty in the estimation of the wall properties described below, and the contact resistance between the probes and the wall. Since the mass method of measuring moisture is considered accurate, the moisture content of bricks for a relative humidity of 0.46% can be considered accurate, while the value determined from the literature is 0.42%, which means an error of 8.6% at this point of the sorption isotherm.

The heat conductivity coefficient was measured with the Isomet 2114 device using a single measurement for every state, the declared accuracy for the range 0.015 . . . 0.70 W/(mK) is 5% of reading + 0.001 W/(mK), and for the range 0.70 . . . 6.0 W/(mK) is 10% of reading.

The water vapor permeability values adopted from [26] according to the authors were measured with an uncertainty of approximately 1%, but the total uncertainty in the derived values can reach 30%, mainly due to the inhomogeneity of the materials. The actual value of the wall tested was not analyzed. It seems that the uncertainty of this parameter is the highest.

## 3. Results

All calculations were performed in an Excel spreadsheet created for this purpose. The results' presentation was also divided into structure composition results and heat and moisture fluxes.

### *3.1. Structural Research*

Figure 6a,b show images of the granular structure of the brick taken using a scanning electron microscope (Section 2.2). Capillary holes with a size of 4–6 µm are visible, so according to the IUPAC classification, these are macropores. These pore structure sizes correspond to the pore size distributions for the ceramic bricks determined in [28].

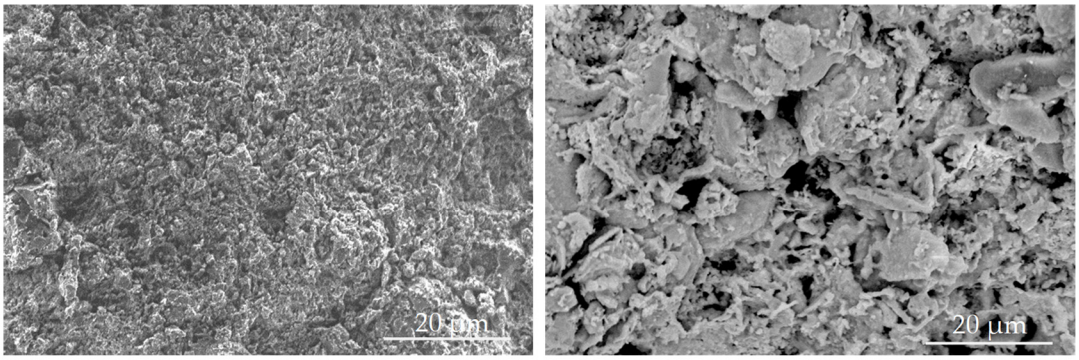


**(a)** **(b)**

**Figure 6.** SEM image of a solid brick from the studied wall; (**a**,**b**) magnification 5000×.

Figure 6 clearly shows that the brick structure is not uniform. Research carried out using a scanning electron microscope, in addition to fragments of brick with a smaller grain size and a compact structure practically devoid of micropores (Figure 6a), also showed areas with a larger grain size, reaching up to 25 µm, and a less compact structure with numerous pores (Figure 6b).

### *3.2. Elemental Composition Studies*

Using a compressed EDX detector with a Quanta 250 FEG FEI microscope, the elemental composition of the brick was examined in five areas, namely A, B, C, D, and E (Figure 7, corresponding visually to various material features on the brick surface. A

total of 18 measurements were made, 3–5 for each analyzed area. Area C corresponded to a compact structure (Figure 7), and areas A, B, D, and E were characterized by greater granularity (Figure 7). The obtained percentage elemental compositions turned out to be similar; however, in the place of the compact structure, an approximate 3–5 times increase in the amount of calcium was observed (respectively, for the areas: A: 4.00%, B: 6.92%, C: 7.77%, D: 20.48%, E: 4.49%). The average test results are presented in Figure 7.

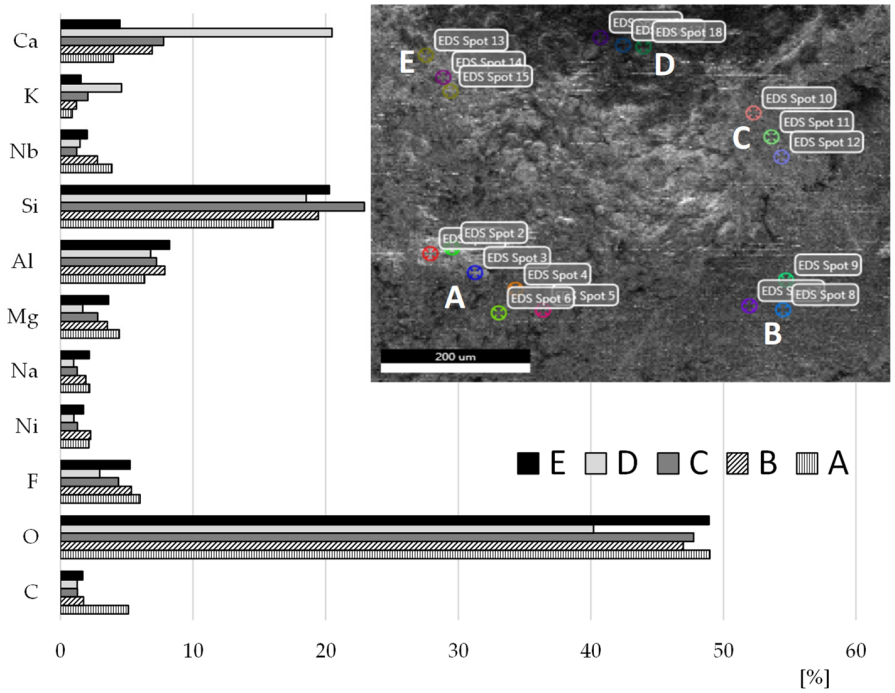


**Figure 7.** Areas analyzed for elemental composition presented in the form of a column chart averaged for a given area.

### *3.3. Measurement of Ambient Temperature and Relative and Absolute Humidity*

The measurements were carried out on the outer (Figure 8a–f) and inner (Figure 9a–f) sides of the wall. Temperature measurements (Figures 8a,b and 9a,b) and relative humidity (Figures 8c,d and 9c,d) performed in the period 5–30 August 2023 (Figures 8a,c,e and 9a,c,e) and 1–30 January 2024 (Figures 8b,d,f and 9b,d,f). The absolute humidity (Figures 8c,f and 9c,f) was calculated from temperature and relative humidity. The months of August and January were selected for further analysis because there was a heat wave in August, while January was the coldest month of winter in 2023/2024.

In January, the average outdoor relative humidity was 88.4%, although the absolute humidity was only 3.5 g/kg. In August, the relative humidity was 68.4%, with an absolute humidity of 11.2 g/kg. Inside, in January, the average relative humidity was 29.1%, with an absolute value of 5.0 g/kg, and in August, it was 59.3% and 11.2 g/kg. Despite the higher moisture content in winter, the relative humidity in the interior was low due to heating and, in addition, water vapor outflow through the wall. In the course of the external temperature in summer, daily variability is more pronounced, and while the internal temperature in summer and winter is equal, it seems that the thermal capacity of the basement walls together with the ground is decisive here.

### *3.4. Temperature and Humidity Inside the Wall*

Table 6 shows the minimum and maximum temperature and relative humidity values for January and August in specific points in the wall.

### *3.5. Results of Heat and Moisture Fluxes on a Daily and Monthly Scale*

The average daily values obtained for horizontal heat fluxes $q_{h,0.25,0.35}$ and $q_{h,0.45,0.35}$ and vertical $q_{h,0.16,0.35}$, $q_{h,-0.16,0.35}$ in August are shown in Figure 10. The stream $q_{h,0.45,0.35}$, i.e., close to the outer side of the wall, shows large fluctuations in value and direction, while on the inner side $q_{h,0.25,0.35}$, these changes are smaller. There is apparently a large increase in heat input during the 13–17 August heat wave. The vertical flux $q_{h,0.16,0.35}$ from the upper parts of the wall is comparable to the flux from the inner side of the wall. However, the flux between the part buried in the ground $q_{h,-0.16,0.35}$ is much smaller than that exchanged through the wall in contact with the outside air. During high temperatures, horizontal heat flow is visible inside the room and vertical flow from the foundations to the upper floors of the building. The direction of vertical flow may be caused by the slower heating of the connection between the wall and the basement ceiling than the part of the wall below. When the outside temperature drops, the flow is reversed.

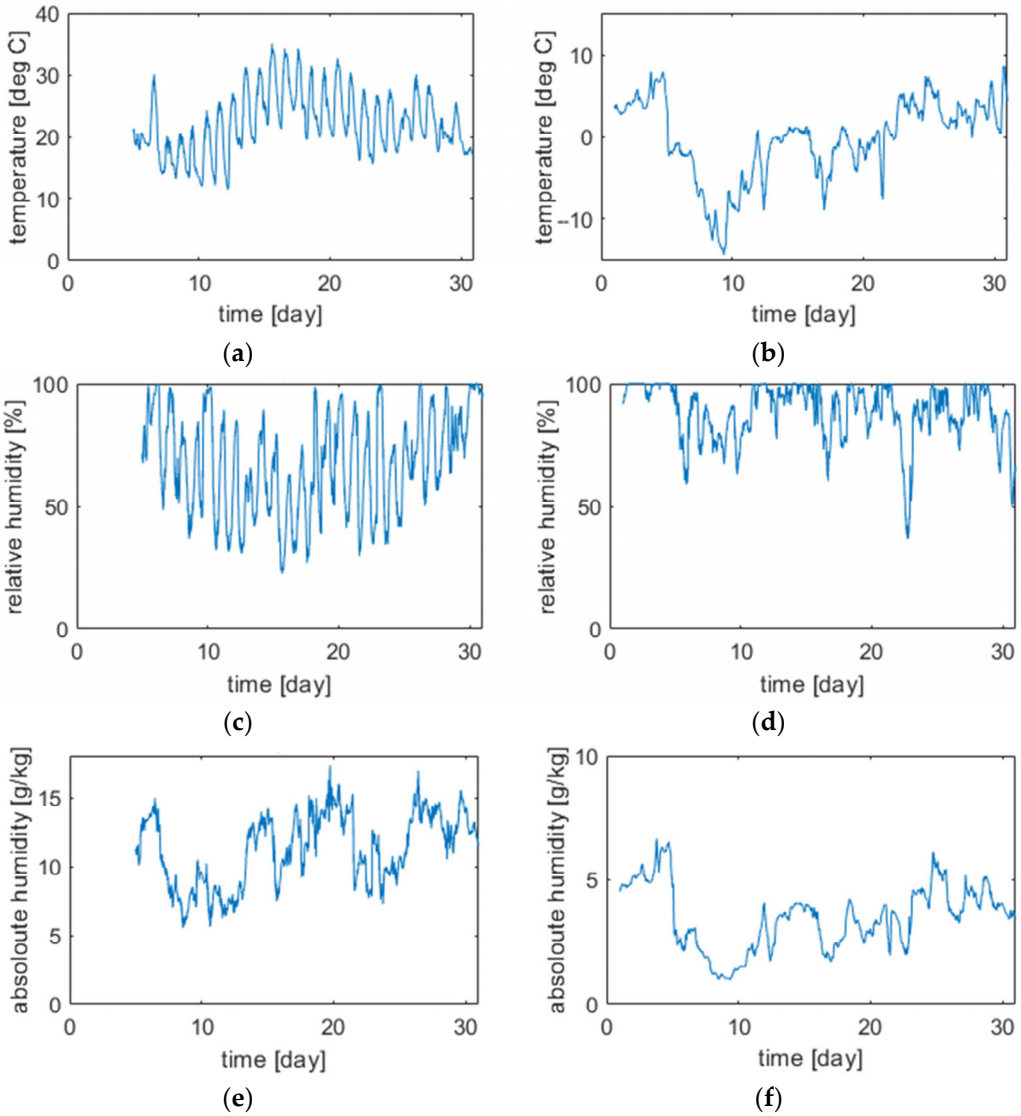


**Figure 8.** External parameters August: (**a**) temperature, (**c**) relative humidity, (**e**) absolute humidity. January: (**b**) temperature, (**d**) relative humidity, (**f**) absolute humidity.

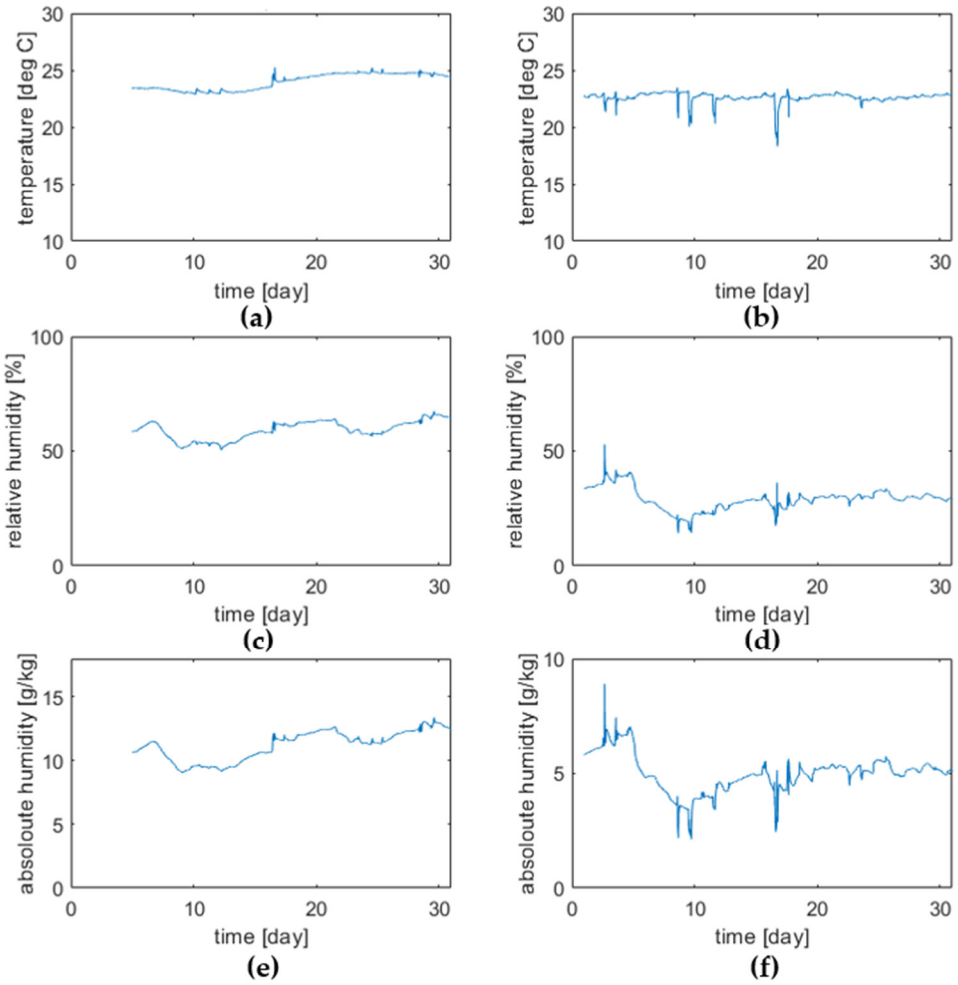


**Figure 9.** Internal parameters August: (**a**) temperature, (**c**) relative humidity, (**e**) absolute humidity. January: (**b**) temperature, (**d**) relative humidity, (**f**) absolute humidity.

**Table 6.** Values of minimum and maximum temperature and relative humidity for January and August.

| Parameter | Month | Min/Max | Distance from the Inner Surface of the Wall [m] | | |
|---|---|---|---|---|---|
| | | | **0.25** | **0.35** | **0.45** |
| Temperature [°C] | January | Max | 16.94 | 15.59 | 14.19 |
| | | Min | 12.42 | 9.63 | 4.77 |
| | August | Max | 27.10 | 27.72 | 29.57 |
| | | Min | 22.26 | 21.68 | 20.32 |
| Relative humidity [%] | January | Max | 47.74 | 51.35 | 57.89 |
| | | Min | 43.99 | 48.42 | 51.84 |
| | August | Max | 53.26 | 53.71 | 55.08 |
| | | Min | 50.23 | 49.07 | 48.36 |
| Partial pressure of steam [Pa] | January | Max | 916 | 900 | 930 |
| | | Min | 659 | 580 | 446 |
| | August | Max | 1908 | 1997 | 2247 |
| | | Min | 1353 | 1278 | 1159 |

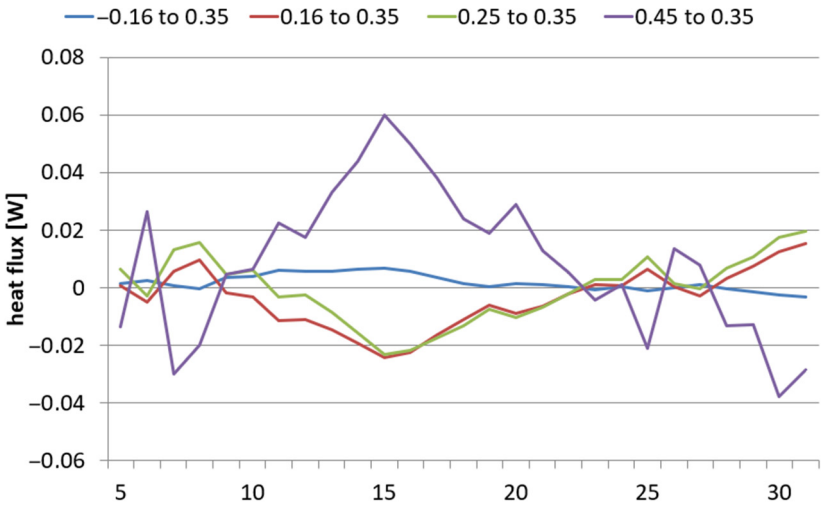


**Figure 10.** Average daily heat fluxes between nodes in August (5 August–31 August).

Water vapor streams are shown in Figure 11.

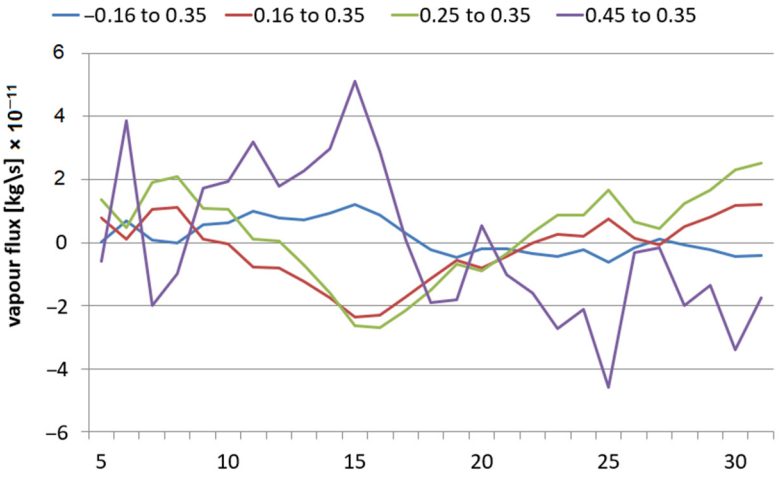


**Figure 11.** Average daily water vapor fluxes between nodes in August (5 August–31 August).

The directions of the vapor flows are similar to those of the heat flows. After the outside temperature drops, the flow penetrating the wall decreases faster than in the case of heat. It is probably related to the persistently high absolute humidity of the external air (Figure 9e).

In the cold season, shown in Figure 12, the horizontal flow of heat in the wall is more orderly and directed outward, while the vertical flow takes place from the upper parts of the building to the foundations.

Noteworthy is the similarity of the course of horizontal streams $q_{h,0.25,0.35}$ and vertical streams $q_{h,0.16,0.35}$, and while the values $q_{h,0.45,0.35}$ and $q_{h,-0.16.0,35}$ also have similar shapes, it is not visible in the chart due to the scale. This second pair of streams is forced by similar temperature differences, but instead of the outside air temperature, the ground temperature occurs.

Figure 13 shows horizontal and vertical moisture fluxes in January.

Water vapor flows from the internal to the external environment and from the top to the bottom of the building. Unlike in the case of heat fluxes, there is a visible similarity between horizontal and vertical fluxes. The absolute values of both heat and moisture fluxes in summer and winter are similar, but in winter, the horizontal and vertical fluxes, respectively, are much closer to the steady state.

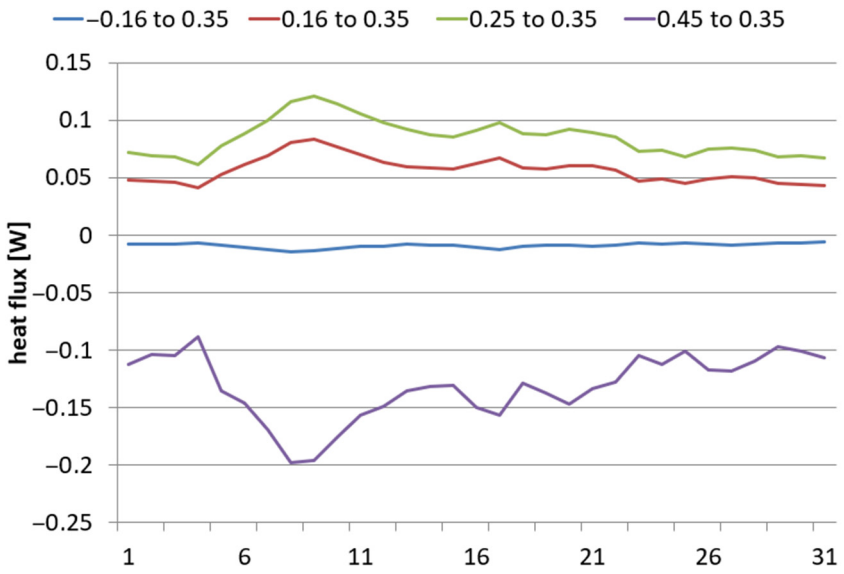


**Figure 12.** Average daily heat fluxes between nodes in January (1 January–31 January).

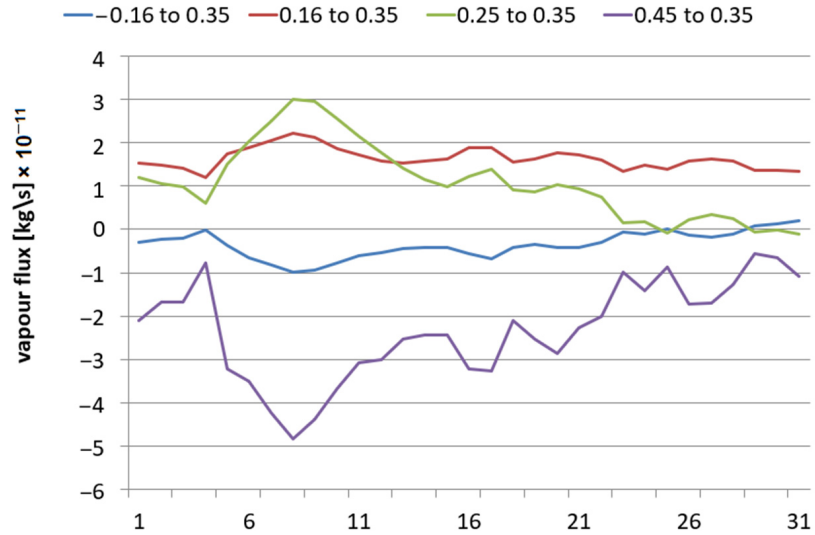


**Figure 13.** Average daily water vapor flows between nodes in January (1 January–31 January).

The monthly energy and moisture flows are listed in Tables 7 and 8, respectively. Measurements started on 5 August; therefore, the flows for January were summed in the range of 5–30 January to maintain comparability.

**Table 7.** Monthly heat flows.

| Energy [J/month] | Measurement | Steady State | Measurement | Steady State |
|---|---|---|---|---|
| | August | | January | |
| $q_{h,-0.16,0.35}$ | 4285 | | −21,375 | |
| $q_{h,0.16,0.35}$ | −8834 | | 136,574 | |
| $q_{h,0.25,0.35}$ | −1278 | 33,115 | 204,046 | 407,840 |
| $q_{h,0.45,0.35}$ | 20,249 | −33,115 | −316,935 | −407,840 |

**Table 8.** Monthly vapor flows.

| Moisture [kg/month] | Measurement | Steady State | Measurement | Steady State |
|---|---|---|---|---|
| | August | | January | |
| $q_{v,-0.16,0.35}$ | $3.213 \times 10^{-6}$ | | $-8.854 \times 10^{-6}$ | |
| $q_{v,0.16,0.35}$ | $-5.009 \times 10^{-6}$ | | $3.885 \times 10^{-5}$ | |
| $q_{v,0.25,0.35}$ | $6.442 \times 10^{-6}$ | $7.81 \times 10^{-7}$ | $2.583 \times 10^{-5}$ | $3.86 \times 10^{-5}$ |
| $q_{v,0.45,0.35}$ | $-1.768 \times 10^{-6}$ | $-7.81 \times 10^{-7}$ | $-5.682 \times 10^{-5}$ | $-3.86 \times 10^{-5}$ |

The uniformity of streams in winter is visible by comparing the amount of energy, and although the range of variability during the month is similar, the rate of change over time is much slower. In summer, negative and positive flows become zero, giving a small monthly total. In August, energy flowed vertically from the foundations to the upper part of the wall, while horizontally from the outside to the inside of the building, and in January the direction of the flows was reverse. In steady-state calculations taking into account only air temperatures, heat always transfers from inside to outside. In August, heat gains flowing towards node 0.25 constitute only 6% of the gains flowing from node 0.45. In winter, the heat flux from node 0.25 to 0.35 is 64% of the flux from 0.35 to 0.45 and probably beyond. In the outer layers of the wall, heat exchange is much more intense, especially in summer. Heat losses from the room through the wall in winter are much greater than gains in summer.

A graphical summary of energy and moisture flows is presented in Figure 14. The arrows in the figure are proportional to the flow size according to Tables 6 and 7.

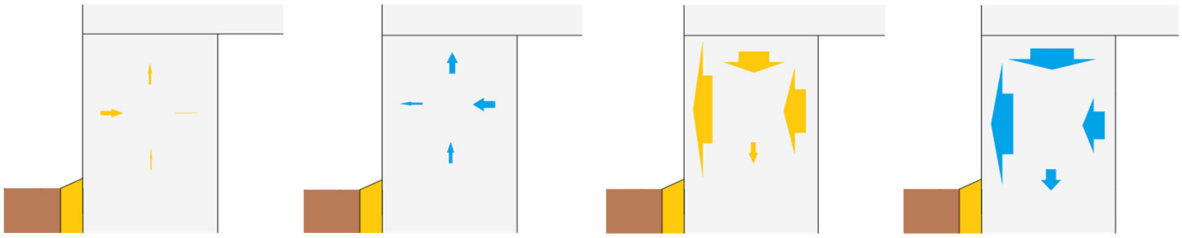

(a) (b) (c) (d)

**Figure 14.** Directions and values of flows in August: (**a**) heat, (**b**) water vapor; January: (**c**) heat, (**d**) water vapor, explanation in text.

Figure 14 shows that the share of vertical energy flows is significant. It is probably smaller in the wall away from the ground and ceilings, but in the analyzed case, two-dimensional calculations should be carried out. In August, the direction of water vapor flow vertically is consistent with the direction of heat flow, while horizontally it is the opposite. The reason for low monthly water vapor flows in summer is similar to that for heat flows, i.e., the positive and negative values become zero. In summer, steam flows in the inner layer of the wall are higher than in the outer layer. In January, the directions of heat and steam flows are consistent. Only a small stream of steam and heat penetrates towards the foundations, which may prove the effectiveness of the insulation.

### *3.6. Hourly Heat and Moisture Fluxes*

To more precisely determine the values and mutual relations of the heat and moisture fluxes, the changes were compared with a recording frequency of 10 min. This comparison was made for a subjectively selected period in the analyzed months. When selecting the representative summer period, high temperatures and low temperatures in winter and their dynamic variability were taken into account. The summer period is 14 August 2023–16 August 2023 and the winter period is 8 January 2024–10 January

2024. Here, too, the positive sign of each heat and moisture flux means flow towards the 0.35 node.

3.6.1. Summer Period

The heat fluxes are shown in Figure 15.

The horizontal stream closest to the outer side of the wall shows the greatest fluctuations. This is consistent with the simulation results [31]. The horizontal stream from the inside $q_{h,0.25,0.35}$ has much smaller changes in value and becomes negative as the outside temperature increases, which means that it flows to the inside room. However, such a flow only occurs during a heatwave, as can be seen in Figure 11. The vertical flow from the upper floors of the building is comparable to the horizontal flow from the inside, while the flow to the foundations is much smaller. The moisture flow diagram is shown in Figure 16.

The variability of the water vapor flow in terms of shape resembles the flow of heat. The stream $q_{v,0.45,0.35}$ shows the largest oscillations, but most of it is positive, i.e., steam flows from the outside of the wall to its center. The vertical flux from the upper floors of the building differs more from the horizontal flux from the inside than in the heat flow, while the flux to the foundations is relatively larger.

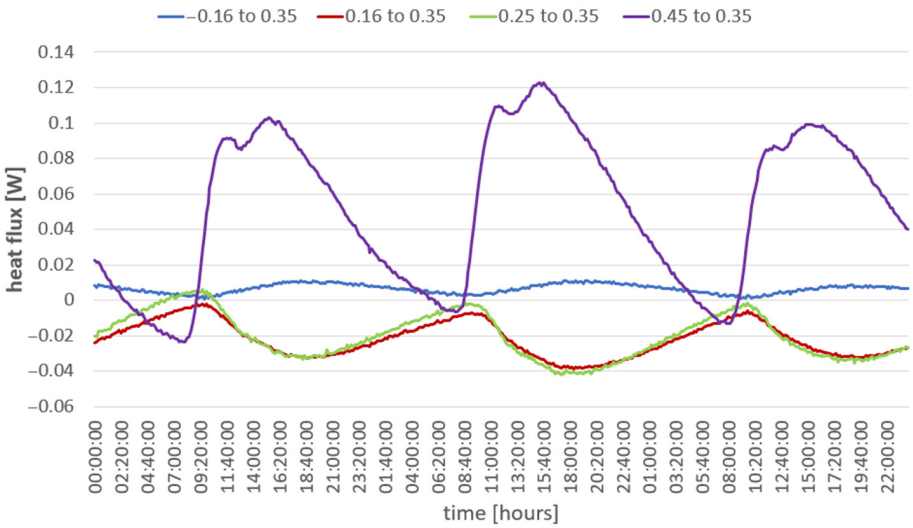


**Figure 15.** Heat flows between nodes on 14 August 2023 and 16 August 2023.

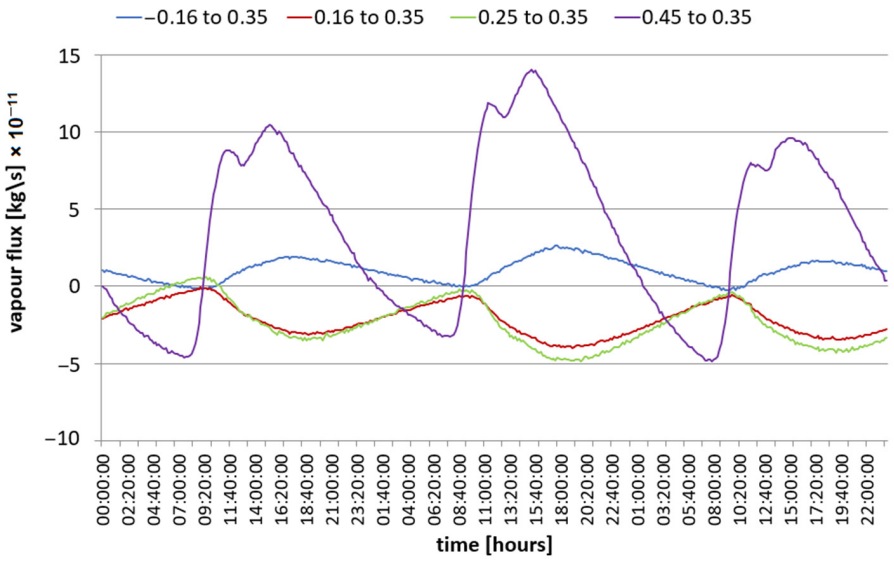


**Figure 16.** Water vapor streams between nodes on 14 August 2023–16 August 2023.

3.6.2. Winter Period

The heat fluxes are shown in Figure 17.

The values of the heat flow streams are more stabilized. At all times, the horizontal heat flow is directed outside the wall and the vertical heat flow towards the foundations. The greatest differences are shown by the flux $q_{h,0.45,0.35}$, and in January it is larger than in August and is directed outwards throughout the entire analyzed period.

The water vapor flow diagram is shown in Figure 18.

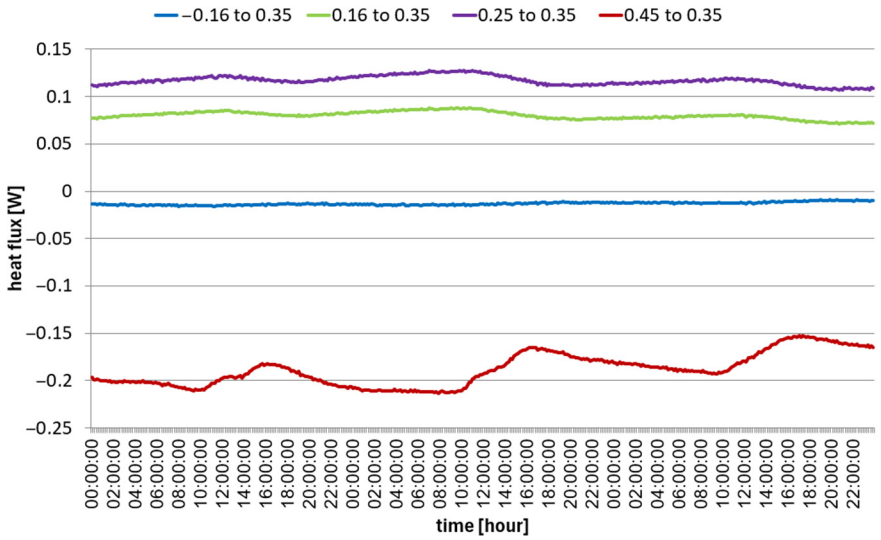


**Figure 17.** Heat flows between nodes on 8 January 2024–10 January 2024.

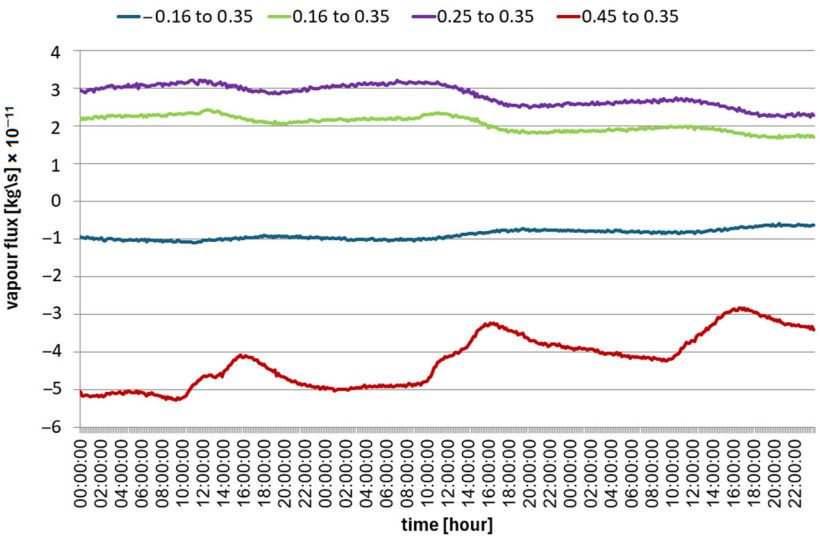


**Figure 18.** Water vapor streams between nodes on 8 January 2024–10 January 2024.

## 4. Discussion

There are many works on benchmark tasks for the calculation of heat and moisture flows [32,33], but they are based on measurements under laboratory conditions. Such experiments are often aimed at explaining some phenomenon, for example, the effect of buffering moisture in a wall on the hygrothermal conditions in a building [34]. At the other extreme, there are "whole building" measurements in natural conditions [35,36]. They aim to record or simulate the thermal and humidity behavior of the entire building, although due to the complexity of the tasks, they are usually simplified. This article deals with measurements under natural conditions on a single wall of a building, which is in the middle of the complexity level.

Publication [13] also examined heat and moisture flows under natural conditions. For an external wall made of 0.2 m of concrete and protected from the inside with a 0.01 m EPS layer and the same thickness of plasterboard, energy flows in August were approx. 0.8 kWh/(m$^2$) towards the room in August kWh/(m$^2$) and 0.27 outside in January, while the moisture flow is 0.1 kg/m$^2$ towards the room in August and 0.16 kg/m$^2$ outside in January. The values from the measurements in this article from Table 6 after conversion are $q_{h,0.25,0.35} = -0.0355$ kWh/m$^2$ and $q_{h,0.45,0.35} = 0.5625$ kWh/m$^2$ in August, and $q_{h,0.25,0.35} = 5.6679$ kWh/m$^2$ and $q_{h,0.45,0.35} = -8.8$ kWh/m$^2$ in January. A thicker wall better retains the heat that comes in in the summer, but room heating and a more severe winter cause much greater losses. The measured moisture fluxes were $q_{v,0.25,0.35} = 0.0006442$ kg/m$^2$ and $q_{v,0.45,0.35} = -0.0001768$ kg/m$^2$ in August and $q_{v,0.25,0.35} = 0.002583$ kg/m$^2$ and $q_{v,0.45,0.35} = -0.005682$ kg/m$^2$ in January. Moisture flows are much smaller, and in summer there is a change in direction; this may be caused by the higher relative humidity in the wall described in [13], and perhaps the flow of capillary water.

Structural tests performed using a scanning electron microscope showed some structural heterogeneity of the brick. This heterogeneity was of a physical nature in the form of porosity and of a chemical nature in the form of elemental composition. In [22], it was shown that the water vapor conductivity coefficient is directly proportional to the porosity of the brick. A higher value of the coefficient results in a more even distribution of water vapor in the wall. The main constituent elements found in the tested brick were also detected, namely Si, Ca, Al, Mg, Na, and K oxides. In this paper, the authors linked the size of micropores with an increase in the permeability of water vapor. Porosity and elemental composition also affect the heat conduction coefficient, but this requires further research. The results obtained for the elemental composition are similar to [24], where the brick was also mainly composed of silica, and the third and fourth elements are calcium and aluminum.

The survey results obtained using a scanning electron microscope showed a rather heterogeneous structure of the brick with visible micropores of approximately 5 μm. The limitations of the research are the heterogeneity of the wall material, the accurate estimation of its properties, and the inaccuracies in the measurement of temperature and humidity. An accurate measurement of wall properties is not possible due to likely local inhomogeneities. In order to obtain truly one-dimensional flows in the future, it would be necessary to consider placing the sensors in one line. This is difficult because of their wiring. Additionally, to accurately measure the temperature, it was necessary to ensure good contact of the sensors with the wall, for example, by using thermal paste, but a layer of such material could disturb the moisture measurement. Similarly, it would be necessary to investigate the possibility of improving the way of measuring external and internal conditions, but these values do not have a great impact on the results because they only served to determine interesting time intervals for research.

## 5. Conclusions

In order to quantitatively estimate the heat fluxes through the wall in solid brick technology near the ground and the ceiling, an analysis of the brick material was performed, revealing its structure and chemical composition. Then, the temperature and relative humidity were measured at selected points in the wall. On the basis of the measurements, horizontal and vertical heat fluxes were calculated in the warm and cold periods of the year. Based on the research, the following conclusions can be drawn:

- The elemental composition of the tested brick includes C, F, Ni, Na, Mg, Si, Nb, K, and Ca. The visually most compact structure has 3–4× more Ca;
- The vertical flow of heat and moisture contributes significantly to the total penetration through the wall under test;
- The fact of heating the room effectively reduces the humidity of the internal air and also inside the wall. The problem of high humidity in rooms with walls in contact with the ground, especially in winter, is described in [5,13];

- An increase in external temperature causes an increase in the partial pressure of steam inside the wall and even a reversal of the flow; this effect is particularly visible in the outer layers of the wall. A similar phenomenon was described in [35] as "sun driven vapor", which may indicate that the heat-insulating plaster has humidity-stabilizing properties by releasing steam when heated;
- The properties of the wall that stabilize the humidity inside the wall are also confirmed by small changes in relative humidity between winter and summer;
- Heat gains through the wall are possible, especially in summer and periodically in winter, but they are small compared to the losses during the year;
- The flux of heat and moisture to foundations is the lowest on record in every case except moisture in August;
- In winter, both moisture and heat flows have lower daily and monthly variability.

**Author Contributions:** Conceptualization, M.O. and B.N.; methodology, M.O. and B.N; investigation, M.O.; data curation, M.O.; writing—original draft preparation, M.O. and B.N; writing—review and editing, M.O. All authors have read and agreed to the published version of the manuscript.

**Funding:** This research received no external funding.

**Data Availability Statement:** The data used in this study are indicated in the text, or contact the first author by email.

**Conflicts of Interest:** The authors declare no conflicts of interest.

## References

1. O'Hegarty, R.; Amedeo, G.; Kinnane, O. The impact of compromised insulation on building energy performance. *Energy Build.* **2024**, *316*, 114337. [CrossRef]
2. Vertaľ, M.; Zozulák, M.; Vašková, A.; Korjenic, A. Hygrothermal initial condition for simulation process of green building construction. *Energy Build.* **2018**, *167*, 166–176. [CrossRef]
3. Calle, K.; Van Den Bossche, N. Towards understanding rain infiltration in historic brickwork, 11th Nordic Symposium on Building Physics. *Energy Procedia* **2017**, *132*, 676–681. [CrossRef]
4. Ramirez, R.; Ghiassi, B.; Pineda, P.; Lourenço, P.B. Hygro-Thermo-Mechanical Analysis of Brick Masonry Walls Subjected to Environmental Actions. *Appl. Sci.* **2023**, *13*, 4514. [CrossRef]
5. Kočí, V.; Kočí, J.; Maděra, J.; Pavlik, Z.; Gu, X.; Zhang, W.; Černý, R. Thermal and hygric assessment of an inside-insulated brick wall: 2D critical experiment and computational analysis. *J. Build. Phys.* **2018**, *41*, 497–520. [CrossRef]
6. Künzel, H.M. Simultaneous Heat and Moisture Transport in Building Components: One– and Two–Dimensional Calculation Using Simple Parameters. Ph.D. Thesis, Fraunhofer Institute for Building Physics, Stuttgart, Germany, 1995.
7. Sasic Kalagasidis, A.; Weitzmann, P.; Nielsen, T.R.; Peuhkuri, R.; Hagentoft, C.-E.; Rode, C. The International Building Physics Toolbox in Simulink. *Energy Build.* **2007**, *39*, 665–674. [CrossRef]
8. Sontag, L.; Nicolai, A.; Vogelsang, S. *Validation of the Solver Implementation of the Hygrothermal Simulation Program DELPHIN*; Technische Universität Dresden: Dresden, Germany, 2013. (In German)
9. Kosny, J.; Kossecka, E. Multi-dimensional heat transfer through complex building envelope assemblies in hourly energy simulation programs. *Energy Build.* **2002**, *34*, 445–454. [CrossRef]
10. dos Santos, G.H.; Mendes, N.; Philippi, P.C. A building corner model for hygrothermal performance and mould growth risk analyses. *Int. J. Heat Mass Transf.* **2009**, *52*, 4862–4872. [CrossRef]
11. Berger, J.; Gasparin, S.; Mazuroski, W.; Mendes, N. An efficient two-dimensional heat transfer model for building envelopes, Numerical Heat Transfer, Part A: Applications. *Int. J. Comput. Methodol.* **2021**, *79*, 163–194. [CrossRef]
12. Berger, J.; Mazuroski, W.; Mendes, N.; Guernouti, S.; Woloszyn, M. 2D whole-building hygrothermal simulation analysis based on a PGD reduced order model. *Energy Build.* **2016**, *112*, 49–61. [CrossRef]
13. Yuan, L.; Takada, S.; Nagano, Y.; Fukui, K. Quantification of moisture flux from the wall surface in contact with the ground in a semi-underground space based on measurements and hygrothermal analysis. *J. Build. Eng.* **2023**, *73*, 106803. [CrossRef]
14. Hens, H. *IEA-ECBCS Annex 41: Whole Building Heat, Air and Moisture Response (LO-09-007)*; ASHRAE Transactions: Louisville, KY, USA, 2009.
15. He, X.; Feng, C.; Zhang, H. Coupled heat and moisture transfer in walls featuring moisture-buffering materials and ventilating layers: An Experimental study. *Energy Built Environ.* **2024**, *5*, 97–109. [CrossRef]
16. Kim, S.-H.; Lee, J.-H.; Kim, J.-H.; Yoo, S.-H.; Jeong, H.-G. The Feasibility of Improving the Accuracy of In Situ Measurements in the Air-Surface Temperature Ratio Method. *Energies* **2018**, *11*, 1885. [CrossRef]
17. Huang, S.; Tao, B.; Li, J.; Yin, Z. On-line heat flux estimation of a nonlinear heat conduction system with complex geometry using a sequential inverse method and artificial neural network. *Int. J. Heat Mass Transf.* **2019**, *143*, 118491. [CrossRef]

18. Sassine, E.; Younsi, Z.; Cherif, Y.; Chauchois, A.; Antczak, E. Experimental determination of thermal properties of brick wall for existing construction in the north of France. *J. Build. Eng.* **2017**, *14*, 15–23. [CrossRef]
19. Habib, E.; Cianfrini, M.; de Lieto Vollaro, R. Definition of Parameters Useful to Describe Dynamic Thermal Behavior of Hollow Bricks. *Energy Procedia* **2017**, *126*, 50–57. [CrossRef]
20. Laou, L.; Ulmet, L.; Yotte, S.; Aubert, J.-E.; Maillard, P. Simulation of the Hygro-Thermo-Mechanical Behavior of Earth Brick Walls in Their Environment. *Buildings* **2023**, *13*, 3061. [CrossRef]
21. D'Ayala, D.; Zhu, H.; Aktas, Y. The Impact of Wind-Driven Rain on Surface Waterproofed Brick Cavity Walls. *Buildings* **2024**, *14*, 447. [CrossRef]
22. Dondi, M.; Principi, P.; Raimondo, M.; Zanarini, G. Water vapour permeability of clay bricks. *Constr. Build. Mater.* **2003**, *17*, 253–258. [CrossRef]
23. Siwiński, J.; Szcześniak, A.; Nasiłowska, B.; Mierczyk, Z.; Kubiak, K.; Stolarski, A. Effect of the mix composition with supep plasticizer admixture on mechanical properties of high–strength concrete based on reactive powders. *Arch. Civ. Eng.* **2022**, *68*, 77–95. [CrossRef]
24. Zawrah, M.F.; Gado, R.A.; Feltin, N.; Ducourtieux, S.; Devoille, L. Recycling and utilization assessment of waste fired clay bricks (Grog) with granulated blast-furnace slag for geopolymer production. *Process Saf. Environ. Prot.* **2016**, *103*, 237–251. [CrossRef]
25. Gawin, D.J.; Kosny, J.; Wilkes, K. Thermal Conductivity of Moist Cellular Concrete Experimental and Numerical Study. In Proceedings of the Performance of Exterior Envelopes of Whole Buildings IX, Clearwater, FL, USA, 5–10 October 2004.
26. Kumaran, M.K.; Lackey, J.C.; Normandin, N.; Tariku, F.; van Reenen, D. Heat, air and moisture transport properties of several North American bricks and mortar mixes. *J. Test. Eval.* **2004**, *32*, 383–389. [CrossRef]
27. Garbalińska, H.; Siwińska, A. Sorption isotherms of ceramic bricks, silicate bricks and aerated concrete. *Build. Phys. Theory Pract.* **2007**, *2*, 41–46. (In Polish)
28. Carmeliet, J.; Roels, S. Determination of the Isothermal Moisture Transport Properties of Porous Building Materials. *J. Therm. Envel. Build. Sci.* **2001**, *24*, 183–210. [CrossRef]
29. Tariku, F.; Kumaran, K.; Fazio, P. Transient model for coupled heat, air and moisture transfer through multilayered porous media. *Int. J. Heat Mass Transf.* **2010**, *53*, 3035–3044. [CrossRef]
30. Gawin, D.J.; Kossecka, E. *The WUFI Computer Program and Its Application in Thermal-Humidity Analysis of Building Partitions*; Lodz University of Technology Press: Lodz, Poland, 2007. (In Polish)
31. Owczarek, M. Thermal fluxes and solar energy storage in a massive brick wall in natural conditions, year-round simulation. In Proceedings of the Building Simulation 2023: 18th Conference of IBPSA, Shanghai, China, 4–6 September 2023. [CrossRef]
32. Hagentoft, C.E. *2002b: HAMSTAD—Final Report: Methodology of HAM-Modeling*; Report R-02:8; Chalmers University of Technology: Gothenburg, Sweden, 2002.
33. Talukdar, P.; Osanyintola, O.F.; Olutimayin, S.O.; Simonson, C.J. An experimental data set for benchmarking 1-D, transient heat and moisture transfer models of hygroscopic building materials. Part II: Experimental, numerical and analytical data. *Int. J. Heat Mass Transf.* **2007**, *50*, 4915–4926. [CrossRef]
34. Yoshino, H.; Mitamura, T.; Hasegawa, K. Moisture buffering and effect of ventilation rate and volume rate of hygrothermal materials in a single room under steady state exterior conditions. *Build. Environ.* **2009**, *44*, 1418–1425. [CrossRef]
35. Piota, A.; Woloszyn, M.; Braub, J.; Abelea, C. Experimental wooden frame house for the validation of whole building heat and moisture transfer numerical models. *Energy Build.* **2011**, *43*, 1322–1328. [CrossRef]
36. Hayduk, G.; Kwasnowski, P.; Fedorczak-Cisak, M.; Furtak, M. Expert Measurement System for MLBE (Lesser Poland Laboratory for Energy-Efficient Buildings) building at the Cracow University of Technology. *Sci. Pap. Fac. Electr. Control. Eng.* **2016**, *49*, 41–48.